

Faster strain fluctuation methods through partial volume updates

Sander Pronk¹ and Phillip L. Geissler²

¹*Department of Bioengineering, University of California, Berkeley, 94720 Berkeley, CA, USA*

²*Department of Chemistry, University of California, Berkeley, 94720 Berkeley, CA, USA*

Elastic systems that are spatially heterogeneous in their mechanical response pose special challenges for molecular simulations. Standard methods for sampling thermal fluctuations of a system’s size and shape proceed through a series of homogeneous deformations, whose magnitudes can be severely restricted by its stiffest parts. Here we present a Monte Carlo algorithm designed to circumvent this difficulty, which can be prohibitive in many systems of modern interest. By deforming randomly selected subvolumes alone, it naturally distributes the amplitude of spontaneous elastic fluctuations according to intrinsic heterogeneity. We describe in detail implementations of such “slice moves” that are consistent with detailed balance. Their practical application is illustrated for a random network of cross-linked polymers.

I. INTRODUCTION

Modern intersections of chemistry, biology, and materials science focus attention on systems that are substantially nonuniform in their spatial organization; examples include interfaces, structural elements of the cell such as the cytoskeleton, and systems undergoing phase transitions. Tools of statistical mechanics that could help clarify their structure and function often do not apply straightforwardly or efficiently in the face of such heterogeneity. This paper concerns a class of computational methods that suffer in this way.

Specifically, we address methods for simulating shape fluctuations of elastic materials. Pioneered by Parrinello and Rahman[1] in the context of molecular dynamics, these approaches extended constant pressure simulation techniques and[2, 3], like their predecessors, opened the door for novel computational studies of phase transitions[4, 5, 6, 7]. The basic idea of these approaches is simple to understand: treat the parameters of a system’s overall geometry as fluctuating dynamical variables, on the same footing as molecular coordinates. In practice, it is convenient to isolate changes in box size and shape by introducing scaled (reduced) coordinates, $\bar{r}_i = h_{ij}^{-1} r_j$, where r_j^i is the j -coordinate of the position vector of atom i and h_{ij} is a matrix of d lattice vectors defining the periodically replicated d -dimensional box geometry. Parrinello and Rahman constructed a Lagrangian with fictitious terms involving h_{ij} and its time derivatives, allowing dynamical simulations of a system with fluctuating shape. One can similarly use Monte Carlo simulations to sample the components of h_{ij} from a Boltzmann distribution[2].

The problem with applying these methods to heterogeneous materials is also simple to understand. When h_{ij} changes, so do the physical positions of all atomic coordinates. For example, if one of the basis vectors in h_{ij} defining a rectangular simulation cell is scaled by some factor, the corresponding components of all position vectors r_i become multiplied by the same factor. The stiffness of the resulting motion is determined by the resistance of molecular interactions to these scale and shear transformations. Sampling efficiency is thus determined by the proverbial “weakest link”: If even a small part of the system strongly resists deformation, then a simulation must await rare, transiently softening fluctuations in local structure that facilitate changes in overall geometry. A

system featuring many locally stiff regions becomes nearly intractable, since the likelihood of many rare local fluctuations occurring simultaneously is extremely small.

Random networks of cross-linked semi-flexible polymers provides an apt example of this pathology: the randomly laid down networks that we will discuss have highly variable local densities of cross-links and therefore vary widely in local stiffnesses. This makes the step size of conventional, global strain moves especially slow: the stiff regions persist through the simulation and will be the limiting factor for the maximum strain move size that still has a reasonable acceptance rate.

In this paper we present a technique that can remove these difficulties by allowing heterogeneous deformations. By transforming only part of a system, we avoid hinging fluctuations of the system as a whole on its stiffest parts. We consider such motions as trial moves in a Metropolis Monte Carlo scheme. We term these as “slice moves”, since they proceed by choosing slices of a system that deform, leaving the remainder of the system internally unaffected. In section II, we introduce the method in detail for both constant pressure (NPT) simulations and constant stress simulations, paying careful attention to the requirement of detailed balance. We illustrate the method in section III through application to the elasticity of a random network of cross-linked semi-flexible polymers, and in section IV we conclude.

II. FAST SAMPLING THROUGH PARTIAL VOLUME MOVES

The basic flaw of conventional strain sampling techniques, when applied to nonuniform systems, is their global nature. We localize strain moves in Monte Carlo simulations by choosing thin slices of a system, outside of which intermolecular geometries are undisturbed. Fig. 1 illustrates such a partial volume move. In this two-dimensional example, subvolumes to be deformed are defined by two intersecting swaths. As a trial move, we deform the region v shared by both slices, producing a new subvolume geometry v' . The requirement that regions outside the two slices remain undeformed then uniquely determines transformations within the remaining slice regions (i.e., within one but not both swaths). By choosing the slices’ locations and widths at random, we

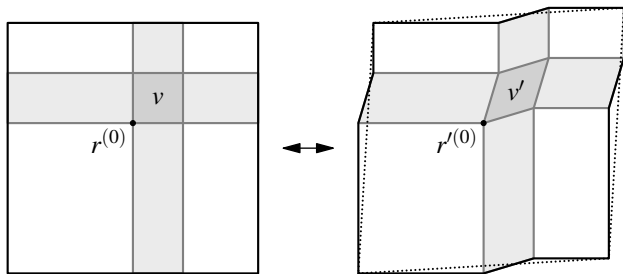


FIG. 1: A partial volume move. The area v transforms to v' , co-transforming the shaded areas. The rest of the simulation box remains unchanged; the new periodically replicating simulation box boundaries are shown as dotted lines.

can in effect sample around problematically rigid parts of a configuration.

Algorithmically, such a “slice move” proceeds as follows:

1. Select a particle at random, whose position $r^{(0)}$ serves as an anchor for the primary deformation subvolume v .
2. Select random parallelepipeds v and v' defining initial and final geometries of the subvolume.
3. Determine additional parallelepipeds $v^{(x)}$, $v^{(y)}$, etc., that connect v with its periodic images (See Fig. 2). These regions, together with v , form the intersecting slices that will be deformed. Repeat for v' .
4. Calculate each particle’s position in the deformed trial state according to strains applied to the region in which it resides.
5. Evaluate the change in internal energy ΔU (accounting for the change in periodic boundary conditions) and the work W associated with external forces.
6. Accept or reject the trial move with a probability determined by the total change in energy relative to $k_B T$

Below we describe two variants of such a trial move. The simpler version involves only the limited class of transformations that switch between rectangular system geometries, for which the shape matrices describing v , v' , h , etc. are all diagonal. The more general, and in practice much more complicated version, includes the possibility of shear deformations as well.

Different periodic images of a particle may move differently in the course of a partial volume move. Detailing the algorithm is therefore greatly simplified by a careful and specific choice of images. Fig. 2 illustrates how we select among each particle’s set of periodically replicated coordinates, according to the subvolume it occupies.

First, we require that each subvolume (v , $v^{(x)}$, $v^{(y)}$, and u) is not fragmented across system boundaries. Since the subvolumes are themselves repeated in space, this criterion does not by itself uniquely specify a choice of particle images. We further choose that the un-fragmented regions are adjacent in

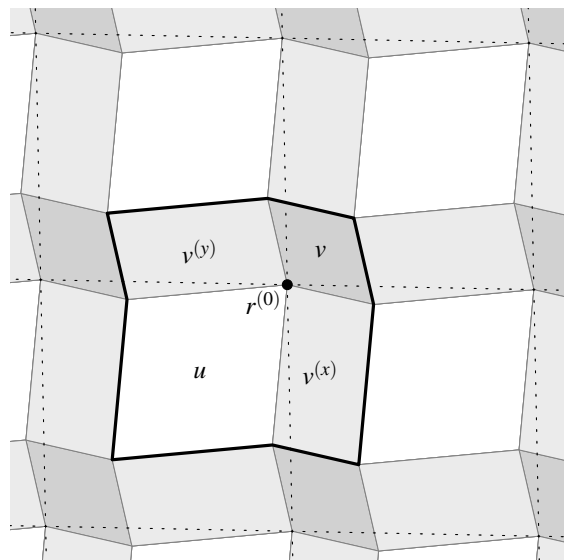


FIG. 2: The connecting subvolumes $v^{(x)}$ and $v^{(y)}$, and the coordinate shifts and periodic boundary conditions during a slice move. The dashed lines show the original periodic boundary box outlined by h_{ij} (already shifted to $r^{(0)}$ at its origin), while the base periodic image during the slice move is shown with the thick lines.

a particular way: the subvolumes $v^{(y)}$, $v^{(x)}$, and u must all contact v , if only at an edge or point, and must contact the anchor point $r^{(0)}$. Note that this scheme results in a collection of particle coordinates that do not lie within the boundary of a single simulation cell. Finally, we translate all particles uniformly so that the anchor point $r^{(0)}$ lies at the origin. While geometrically straightforward, this set of operations carries a nontrivial computational overhead. We describe an efficient implementation in Appendix A.

A. Scaling slice moves in a rectangular simulation box

The simplest slice move is a bulk scaling slice in a rectangular simulation box, as shown in Fig. 3. This corresponds to a volume move in a constant-pressure (NPT) ensemble[8]. In this situation, the box matrix h_{ij} is

$$h_{ij} = l_i \delta_{ij}, \quad (1)$$

where l_i is the size of the system in direction i [11].

After choosing an original slice width v_i , and a new slice width v'_i , the deformation s_i is fixed by

$$v'_i = s_i v_i. \quad (2)$$

Together with the choice of slice origin $r_i^{(0)}$: the location of a randomly selected particle, the move is fixed.

With u_i as the size of the unchanging part of the simulation box, the new box matrix is

$$h'_{ij} = (u_i + v'_i) \delta_{ij}. \quad (3)$$

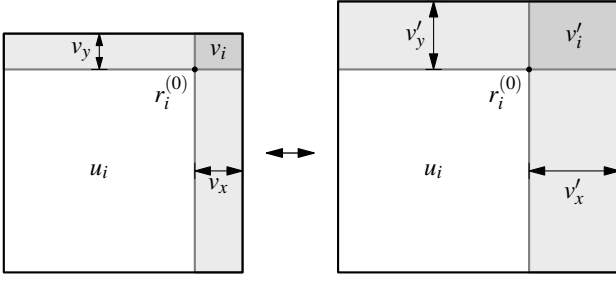


FIG. 3: A partial scaling move in a rectangular box.

Given this deformation, and after shifting the coordinates as described above, and shown in Fig. 2 so that the origin lies at $r_i^{(0)}$, the new location r'_i of a point r_i is

$$r'_i = \begin{cases} s_i r_i & \text{if } r_i > 0, \\ r_i & \text{otherwise.} \end{cases} \quad (4)$$

In practice, it is more convenient to do this transformation in reduced coordinates, where the particles that are outside the slice also move, because of the new box scaling from Eq. 3:

$$\bar{r}'_i = \begin{cases} \Delta h_{ij}^{(\text{int})} \bar{r}_j & \text{if } \bar{r}_j > 0, \\ \Delta h_{ij}^{(\text{ext})} \bar{r}_j & \text{otherwise.} \end{cases} \quad (5)$$

here, the relative deformation matrices $\Delta h_{ij}^{(\text{int})}$ and $\Delta h_{ij}^{(\text{ext})}$ are

$$\Delta h_{ij}^{(\text{int})} = h_{ik}^{-1} s_k h_{kj}, \quad (6)$$

$$\Delta h_{ij}^{(\text{ext})} = h_{ik}^{-1} h_{kj}. \quad (7)$$

The acceptance probability P_{acc} of this move is based on the detailed balance requirement:

$$\frac{\pi(\Gamma')}{\pi(\Gamma)} = \frac{P_{\text{gen}}(\Gamma'|\Gamma) P_{\text{acc}}(\Gamma \rightarrow \Gamma')}{P_{\text{gen}}(\Gamma|\Gamma') P_{\text{acc}}(\Gamma' \rightarrow \Gamma)}, \quad (8)$$

where Γ represents the state of the system, and $\pi(\Gamma)$ its equilibrium probability. The coordinate $r_j^{(i)}$ is the coordinate j of particle number i . The probability P_{gen} can be split into

$$\begin{aligned} P_{\text{gen}}(\Gamma'|\Gamma) &= P\left(r_i^{(1)}, \dots, r^{(N_i)}, h_{ii} \rightarrow r'_i, \dots, r'^{(N_i)}, h'_{ii} \mid v_j, v'_k, r_l^{(0)}\right) \\ &\quad \times P(v_m, v'_n, r_o^{(0)}) \\ &= \prod_{p=1}^d \prod_{i=1}^{N_p} \delta(r_p^{(i)} - s_p r_p^{(i)}) \prod_{j=N_p+1}^{N-1} \delta(r_p^{(j)} - r_p^{(j)}) \\ &\quad \times P(v_m, v'_n, r_o^{(0)}), \end{aligned} \quad (9)$$

where N_p is the number of particles in dimension p , and we've omitted coordinate shifts that have no influence on the probability density.

Note that for notational convenience we've implicitly spatially sorted the particles so that particles $1 \dots N_p$ are in the

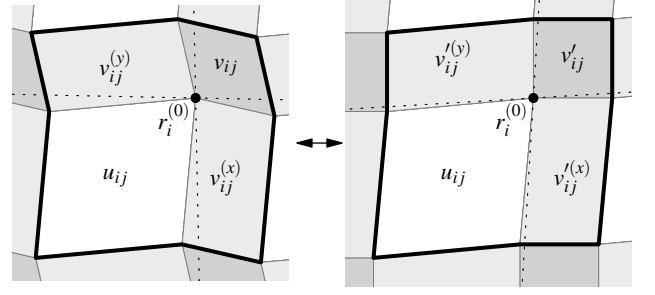


FIG. 4: A partial volume move with shear components. The thick lines represent the is the box boundary as used in the slice move.

slice in the p -direction. Particles $N_p + 1 \dots N - 1$, and the anchor particle 0 are outside the slice. While this sorting cannot be performed for all coordinates simultaneously, it could be done sequentially for each coordinate resulting in the expression above.

The ratio between the forward and backward move generation P_{gen} is

$$\frac{P_{\text{gen}}(\Gamma'|\Gamma)}{P_{\text{gen}}(\Gamma|\Gamma')} = \prod_{p=1}^d \frac{1}{s_p^{-N_p}} \frac{P(v_m, v'_n, r_o^{(0)})}{P(v'_q, v_r, r_s^{(0)})} = \prod_{p=1}^d s_p^{-N_p} \quad (10)$$

where $s'_p = v_p/v'_p = 1/s_p$, and the ratio between the probabilities

$$\frac{P(v_m, v'_n, r_o^{(0)})}{P(v'_p, v_q, r_r^{(0)})} = 1, \quad (11)$$

because v_m and v'_n are chosen independently, and $r_o^{(0)} = r_o^{(0)}$.

Using Eq. 8, the acceptance probability now becomes

$$\begin{aligned} P_{\text{acc}}(v_i, v'_j, r_k^{(0)}) &= \min \left[1, \left(\prod_{p=1}^d \left(\frac{v'_p}{v_p} \right)^{N_p} \right) \right. \\ &\quad \left. \times \exp(-\beta [\Delta \mathcal{H} + \Delta P(|h'_{qr}| - |h_{qr}|)] \right). \end{aligned} \quad (12)$$

where the $|h_{qr}|^N$ term is absent because the move probabilities are formulated in unreduced space: it is subsumed under the $(v'_i/v_i)^{N_i}$ term. In the limit of $v_i \rightarrow h_{ii}$, the acceptance probability becomes equal to $(|h'_{qr}|/|h_{qr}|)^{N-1}$, similar to the normal acceptance ratio for strain moves (here the one remaining factor $|h'_{qr}|/|h_{qr}|$ is missing because the anchor particle is defined to be outside the slices).

B. Slice moves in an arbitrarily shaped simulation box

To incorporate shear components into the slice moves, one cannot just select a rectangular area in the reduced space, as was done in the previous section. As Fig 1 shows, the resulting system would be sheared in the reduced space, making the reverse move impossible.

In order to do a slice move with a shear component correctly, the shape of the slice itself must be allowed to be

a parallelogram-shaped (or parallelepiped-shaped) area, described by a *matrix* v_{ij} , such as shown in Fig. 4, while the unchanged area is described by a matrix u_{ij} . The matrix v_{ij} then gets transformed into an independently chosen matrix v'_{ij} , co-transforming the regions $v_{ij}^{(x)}$ and $v_{ij}^{(y)}$ (in 2D).

All the sections of the simulation box can be described (in 2D) by the quadrant matrices u_{ij} , v_{ij} , $v_{ij}^{(x)}$, $v_{ij}^{(y)}$, together with an anchor particle $r_i^{(0)}$. Like the simulation box matrix h_{ij} , these matrices contain d vectors in row form that together span the area that they describe, or, in other words: the section described by v_{ij} is the linear transform of the unit square (cube) by v_{ij} .

The summed coordinates must add up:

$$h_{ij}\mathbf{1}_j = u_{ij}\mathbf{1}_j + v_{ij}\mathbf{1}_j. \quad (13)$$

where $\mathbf{1}_i$ is the vector with all components equal to 1. This, and similar considerations, lead to

$$u_{ij} = h_{ij} - v_{ij} \quad (14)$$

and

$$v_{ij}^{(k)} = \begin{cases} v_{ij} & \text{if } j = k \\ u_{ij} & \text{otherwise,} \end{cases} \quad (15)$$

and, for 3D systems,

$$v_{ij}^{(kl)} = \begin{cases} v_{ij} & \text{if } j = k \text{ or } j = l \\ u_{ij} & \text{otherwise,} \end{cases} \quad (16)$$

while, after the deformation, the new overall box matrix becomes

$$\begin{aligned} h'_{ij} &= u_{ij} + v'_{ij} \\ &= h_{ij} + (v'_{ij} - v_{ij}) \end{aligned} \quad (17)$$

and the co-transformed parts become

$$v'_{ij}{}^{(k)} = \begin{cases} v'_{ij} & \text{if } j = k \\ u_{ij} & \text{otherwise} \end{cases} \quad (18)$$

(with additional 3D sections as in Eq. 16).

Again, for convenience, we define deformation matrices s_{ij} through

$$s_{ij} = v'_{ik}v_{kj}^{-1}, \quad (19a)$$

$$s'_{ij}{}^{(k)} = v'_{ik}{}^{(k)}(v_{kj}^{(k)})^{-1}, \quad (19b)$$

By making use of the fact that the coordinates of all quadrants (deformation regions) touch the point $r_i^{(0)}$, (as described in section II, and shown in Fig. 2), the coordinates of the deformed system can (in 2D) be written as

$$r'_i = \begin{cases} s_{ij}r_j & \text{if } r_i \text{ is in the } v_{ij} \text{ quadrant,} \\ s_{ij}^{(x)}r_j & \text{if } r_i \text{ is in the } v_{ij}^{(x)} \text{ quadrant,} \\ s_{ij}^{(y)}r_j & \text{if } r_i \text{ is in the } v_{ij}^{(y)} \text{ quadrant,} \\ r_i & \text{if } r_i \text{ is in the } u_{ij} \text{ quadrant.} \end{cases} \quad (20)$$

An efficient algorithm to determine in which quadrant a point r_i falls, is outlined in Appendix A.

The probability to generate this move is similar to that of Eq. 9:

$$\begin{aligned} P_{\text{gen}}(\Gamma'|\Gamma) &= P(v_{ij}, v'_{kl}, r_m^{(0)}) \prod_{p=1}^d \left[\prod_{r=1}^{N_{v^{(x)}}} \delta(r_p^{(r)} - s_{pq}^{(x)}r_q^{(r)}) \right. \\ &\quad \times \prod_{s=N_{v^{(x)}}+1}^{N_{v^{(x)}}+N_{v^{(y)}}} \delta(r_p^{(s)} - s_{pq}^{(y)}r_q^{(s)}) \\ &\quad \times \left. \prod_{t=N_{v^{(x)}}+N_{v^{(y)}}+1}^{N_{v^{(x)}}+N_{v^{(y)}}+N_v} \delta(r_p^{(t)} - s_{pq}r_q^{(t)}) \right] \\ &\quad \times \prod_{u=N_{v^{(x)}}+N_{v^{(y)}}+N_v+1}^{N-1} \delta(r_p^{(u)} - r_p^{(u)}), \end{aligned} \quad (21)$$

where again, we've omitted simple coordinate shifts. N_v , $N_{v^{(x)}}$, and $N_{v^{(y)}}$ are the number of particles in the v , $v^{(x)}$, and $v^{(y)}$ regions, respectively. Like in Eq. 9, the particles are numbered according to the region they are in: particles with index in $1, \dots, N_{v^{(x)}}$ are the particles in $v^{(x)}$; particles with index in $N_x + 1, \dots, N_{v^{(x)}} + N_{v^{(y)}}$ are the particles in $v^{(y)}$, et cetera.

As in Eq. 10, the ratio of backward and forward probabilities becomes:

$$\begin{aligned} \frac{P_{\text{gen}}(\Gamma'|\Gamma)}{P_{\text{gen}}(\Gamma|\Gamma')} &= |s_{ij}^{(x)}|^{-N_{v^{(x)}}} |s_{ij}^{(y)}|^{-N_{v^{(y)}}} |s_{ij}|^{-N_v} \\ &= |v'_{ik}{}^{(x)}(v_{kj}^{(x)})^{-1}|^{-N_{v^{(x)}}} |v'_{ik}{}^{(y)}(v_{kj}^{(y)})^{-1}|^{-N_{v^{(y)}}} |v'_{ik}v_{kj}^{-1}|^{-N_v}, \end{aligned} \quad (22)$$

where, as in the previous section, we assume that we have selected v_{ij} and v'_{ij} independently. Given these conditions, the acceptance probability becomes (again, similar to Eq. 12):

$$\begin{aligned} P_{\text{acc}}(v_{ij}, v'_{kl}, r_m^{(0)}) &= \min \left[1, |s_{mn}|^{N_{v^{(x)}}} |s_{mn}|^{N_{v^{(y)}}} |s_{mn}|^{N_v} \right. \\ &\quad \times \left. \exp(-\beta[\Delta\mathcal{H} + E_d(h'_{op}) - E_d(h_{op})]) \right], \end{aligned} \quad (23)$$

where $E_d(h_{op})$ is the energy associated with system shape h_{op} (usually $P|h_{op}|$), and the anchor particle $r^{(0)}$ is defined to be in the region u_{ij} .

C. Selecting v and v'

In Eq 23, it is again (as in Eq. 11) assumed that the choice of v_{ij} and v'_{ij} is reversible:

$$\frac{P(v_{ij}, v'_{kl}, r_m^{(0)})}{P(v'_{no}, v_{pq}, r_r^{(0)})} = 1, \quad (24)$$

which means that in the simplest case this choice cannot depend on the current shape h_{ij} . The most obvious way of selecting v_{ij} and v'_{ij} would be to select random matrix elements for both matrices (within a certain range). This, however, suffers from a practical acceptance probability problem; while it is desirable to select both matrices from a relatively wide range of possible matrices, v_{ij} and v'_{ij} should not differ too much from each other, as this will make the move rejection ratio too low (strain fluctuations are generally very small).

One simple way to achieve both goals is to first select an intermediary matrix

$$\hat{v}_{ij} = \begin{pmatrix} \text{rnd}(\hat{v}_{xx}^{\min}, \hat{v}_{xx}^{\max}) & \text{rnd}(-\hat{v}_{xy}^{\min}, \hat{v}_{xy}^{\max}) \\ \hat{v}_{yx} & \text{rnd}(\hat{v}_{yy}^{\min}, \hat{v}_{yy}^{\max}) \end{pmatrix}, \quad (25)$$

where $\text{rnd}(a, b)$ is a random number between a and b , chosen with a flat probability distribution. We can now choose v_{ij} and v'_{ij} by selecting a random offset

$$v_{ij} = \hat{v}_{ij} + \Delta v_{ij} = \hat{v}_{ij} + \begin{pmatrix} \text{rnd}(-\delta_{xx}, \delta_{xx}) & \text{rnd}(-\delta_{xy}, \delta_{yx}) \\ \Delta v_{yx} & \text{rnd}(-\delta_{yy}, \delta_{yy}) \end{pmatrix}, \quad (26a)$$

$$v'_{ij} = \hat{v}_{ij} + \Delta v'_{ij} = \hat{v}_{ij} + \begin{pmatrix} \text{rnd}(-\delta_{xx}, \delta_{xx}) & \text{rnd}(-\delta_{xy}, \delta_{yx}) \\ \Delta v'_{yx} & \text{rnd}(-\delta_{yy}, \delta_{yy}) \end{pmatrix}, \quad (26b)$$

so that the acceptance ratio can be controlled by the size of δ_{xx} , δ_{xy} and δ_{yy} , and matrix symmetry is maintained.

The only requirements for the parameters v_{ij}^{\min} , v_{ij}^{\max} , and δ_{ij} is that they are fixed, and that they produce slices that are smaller than the system size. Because overall strain fluctuations are generally small, this should be easily achievable.

Another choice is to choose rectangular slices out of reduced coordinate space for localized expansion and contraction moves similar to Section II A. We start again with an intermediary matrix

$$\hat{v}_{ij} = \begin{pmatrix} \text{rnd}(\hat{v}_{xx}^{\min}, \hat{v}_{xx}^{\max}) & 0 \\ 0 & \text{rnd}(\hat{v}_{yy}^{\min}, \hat{v}_{yy}^{\max}) \end{pmatrix}, \quad (27)$$

and because of the h_{ij} matrix symmetry requirements, make v_{ij} and v'_{ij}

$$v_{ij} = \hat{v} \begin{pmatrix} \hat{v}_{xx} + \Delta v & \frac{h_{xy}}{h_{yy}} (\hat{v}_{yy} + \Delta v) \\ \frac{h_{yx}}{h_{xx}} (\hat{v}_{xx} + \Delta v) & \hat{v}_{yy} + \Delta v \end{pmatrix}, \quad (28a)$$

$$v'_{ij} = \begin{pmatrix} \hat{v}_{xx} + \Delta v' & \frac{h_{xy}}{h_{yy}} (\hat{v}_{yy} + \Delta v') \\ \frac{h_{yx}}{h_{xx}} (\hat{v}_{xx} + \Delta v') & \hat{v}_{yy} + \Delta v' \end{pmatrix}, \quad (28b)$$

where

$$\Delta v = \text{rnd}(-\delta_r, \delta_r), \quad (29a)$$

$$\Delta v' = \text{rnd}(-\delta_r, \delta_r). \quad (29b)$$

The advantage of slices that are rectangular in the reduced coordinate space is that determining which slice a coordinate

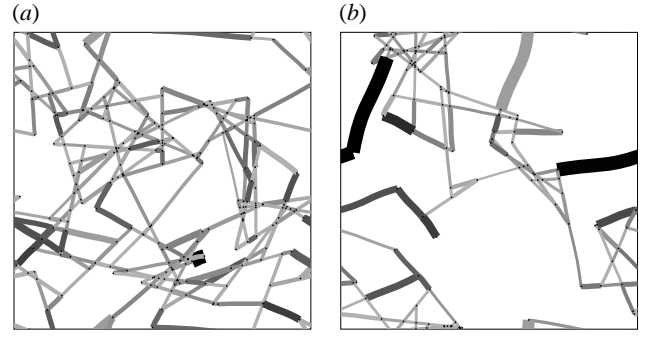


FIG. 5: Two randomly laid down networks of model actin filaments during a Monte Carlo simulation. The line widths denote instantaneous parallel strain for the segment, while the darkest shades denote higher instantaneous perpendicular strain for the segment. The sizes of the systems are $0.25l_p \times 0.25l_p \approx 2.5 \mu\text{m} \times 2.5 \mu\text{m}$, where l_p is the persistence length of actin. System a shows a medium density system (with average distance between cross-links $l_c = 0.014l_p$), while the b shows a low density system (with $l_c = 0.019l_p$). Both have rigid cross-links, and average filament length $0.11l_p$ before removal of free end-points.

is in is much faster than for the general method, resulting in considerable speedup of slice moves.

By combining these moves with the general moves described above, with either $\delta_{xx} = \delta_{yy} = 0$, or $\delta_{xy} = 0$, we can sample all strain states efficiently, with tunable acceptance rate.

III. SIMULATIONS

In order to check whether the slice moves result in an actual speed-up of sampling, we have performed simulations on a locally anisotropic elastic material: a model of the actin cytoskeleton consisting of a randomly laid down 2D network of semi-flexible filaments, linked by floppy or rigid cross-links[9], as shown in Fig. 5.

The filaments in the model bend through thermal fluctuations and in response to imposed stresses, with an energy cost described by the worm-like chain energy[10].

Because the elastic behavior of the network is determined by the cross-links and the effective interactions between them, as mediated through the filaments, we have developed a coarse-grained model of the filaments where the filament itself is replaced by an effective free energy between the cross-links. The cross-links contain the positions and orientations of the points along the two filaments that intersect.

The effective free energy is a free energy of the worm-like chain model, given the positions, orientations, and contour length of the end-points of a filament. Using this free energy as a Hamiltonian, fluctuations of the system are sampled using a standard Metropolis Monte Carlo simulation. This resulting free energy is highly non-linear because of the in-extensibility of the worm-like chain, which causes the interactions between cross-links to be much like those of hard particles, and makes direct calculation of the stress tensor numerically challenging:

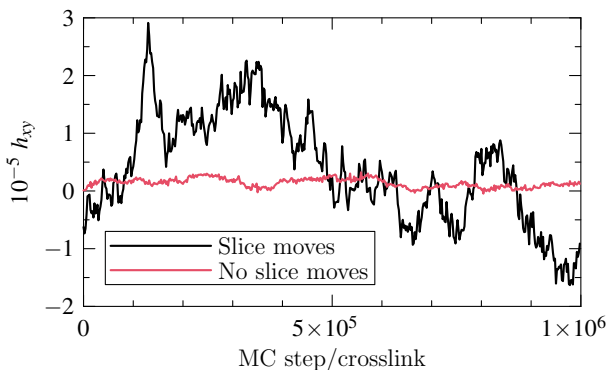


FIG. 6: Shear component h_{xy} during a MC simulation under zero pressure, with and without slice moves. The simulated network is shown is the left configuration of Fig 5.

elastic properties of this system are therefore more easily calculated using strain fluctuation methods.

In Fig 6 we show the results of a simulation on the system shown in Fig. 5a: the shear component of the box matrix h_{xy} as a function of the MC step number. The slice shapes v_{ij} and v'_{ij} were chosen according to the recipe in Section II C, with sizes between 5% – 20% of the full system size (i.e. \hat{v}_{xx}^{\min} and \hat{v}_{yy}^{\min} are 0.05 times the initial box matrix components h_{xx} and h_{yy} , while \hat{v}_{xx}^{\max} and \hat{v}_{yy}^{\max} are 0.2 times the initial box matrix components). The individual shear step size δ_{xy} is around 10^{-7} . All step sizes are tuned during an equilibration phase of the simulation to have an acceptance rate of approximately 0.5.

It is clear that the slice moves not only allow for fast sampling of regions that would otherwise be virtually inaccessible within reasonable CPU time, but that the apparent size of the fluctuations is now much different, leading to a very different shear elastic constant.

For the system shown in Fig 5b, we show what happens if the system is not able to withstand an applied pressure. The cytoskeletal network model used can collapse through buckling; the results of this are shown in Fig. 7: the bulk component h_{xx} shows no signs of having reached equilibrium after 10^7 MC steps per cross-link with slice moves, while in the absence of slice moves the collapse is far less obvious.

The slice moves in constant stress simulations are not without cost, however: a slice move in an arbitrarily shaped simulation box with slices that are not rectangular in the reduced coordinate space can be significantly slower than regular strain moves. The relative computational cost of this is a function of the complexity of the inter-particle potential: as calculating a potential takes longer, less time is spent (relatively) on calculating which slice a point is in.

This drawback does not necessarily apply to *NPT* simulations: here the v_{ij} and v'_{ij} regions are always chosen in such a way that they are rectangular in the reduced coordinate space, making the algorithm that decides which slice a point is in trivial.

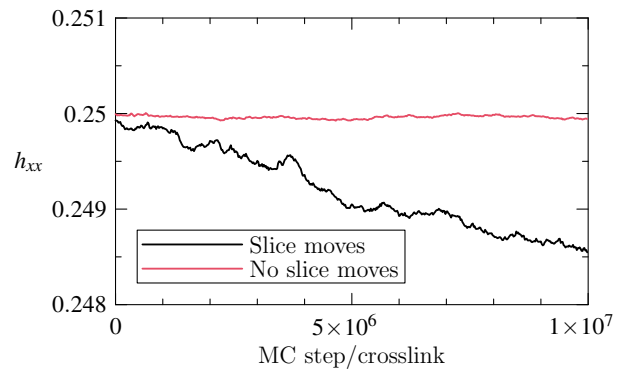


FIG. 7: Bulk component h_{xx} during a MC simulation under applied pressure for a network undergoing collapse through buckling, with and without slice moves. The simulated network is the right configuration of Fig 5.

IV. CONCLUSION

We have shown how volume moves in *NPT* simulations and strain moves in constant-stress simulations can be localized, allowing for significant speedups of MC simulations. The simulation examples showed that strain states that were previously practically inaccessible in elastically heterogeneous systems are now accessible, which enables the application of strain fluctuation methods for inhomogeneous systems, such as those found in biological systems, and systems with large density fluctuations, such as during phase transitions.

This work is supported in part by the California Institute for Quantitative Biosciences, and by the National Science Foundation.

APPENDIX A: ALGORITHM TO DETERMINE WHICH SLICE A POINT IS IN

Every slice move involves determining which slice each particle is in, before transforming the coordinates accordingly (as given by Eqs. 4 and 20). While doing this efficiently with slices that are rectangular in the reduced coordinate space is not complicated, this problem is potentially computationally very costly for non-rectangular slices. Here we describe an algorithm that will reduce this problem to checking whether a point is in a rectangle for most points in the simulation box.

Suppose we want to check in which slice the coordinate r_i is; because coordinates are stored internally in reduced coordinates, and the periodic boundary conditions are simple to express in reduced coordinates, we will use the reduced coordinates \bar{r}_i .

The slices consist of their parallelogram (or parallelepiped) shape parameters, given by the shape matrix μ_{ij} (where $\mu \in \{u, v, v^{(x)}, v^{(y)}\}$ in 2D), and their origin location, determined by $\bar{r}_i^{(0)}$.

The simplest optimization is to pre-calculate a list of the inscribed rectangles of all the slices. Each coordinate can

then be checked quickly against these rectangles, and because strain fluctuations tend to be small, most coordinates will fall within one of these rectangles.

Because the simulation box contains periodic images of the slices, and each particle needs to be checked against each slice in the worst case, it is efficient to limit the number of periodic images. The optimum way to do this is to shift the coordinates of the slice to the center, and shift the coordinates before each check.

This leads to the following algorithm:

1. Pre-calculate the inscribed rectangles \bar{R}^μ for each slice $\mu \in \{u, v, v^{(x)}, v^{(y)}, \dots\}$.
2. Pre-calculate the list $L^{\mu,c}$ of center coordinates and matrices for each slice.
3. For each slice with shape matrix μ_{ij} , determine whether offsetting by a periodic image of the simulation box by $p_i \in \{-1, 0, 1\}$, puts any of its corners into the base periodic image:

$$-\frac{1}{2} \leq h_{ij}^{-1} \mu_{jk} \left[\left(\pm \frac{1}{2}, \pm \frac{1}{2} \right)_k + p_k \right] < \frac{1}{2}, \quad (\text{A1})$$

or that the any of the corners of the base periodic image are in the slice:

$$-\frac{1}{2} \leq \mu_{ij}^{-1} h_{jk} \left(\pm \frac{1}{2}, \pm \frac{1}{2} \right)_k - p_i < \frac{1}{2}, \quad (\text{A2})$$

and if that is the case, add that periodic image to the list of slices from step 2: $L^{\mu,c}$, to check.

4. For each particle coordinate \bar{r}_i :

- (a) Check whether the coordinate falls any of the rectangles \bar{R}^μ . If it does, the coordinate must be in slice μ .
- (b) Check whether the coordinate falls inside any of the slice parallelograms in the list $L^{\mu,c}$ with shape matrix μ_{ij} and center (in reduced coordinates) \bar{c}_k by checking whether

$$-\frac{1}{2} \leq \mu_{ij} h_{jk} \left[\left(\bar{r}_k \dot{-} \bar{c}_k \right) + p_k \right] < \frac{1}{2}, \quad (\text{A3})$$

where p_k are the periodic image offsets from step 3, which are (0,0) for any of the center coordinates added in step 2. The operator $\dot{-}$ denotes a subtraction for which the results are put back into the base periodic image.

By ordering the slice size from smallest to largest in the first three steps, we can ensure that most coordinates are found quickly. Once it has been determined in which slice particles belong, the energy of the new system can be calculated by calculating the change in energy for all particles that have been affected by the slice move. Note that this also includes interactions between particles in the unchanging part of the system u_{ij} that interact through the slice.

[1] M. Parrinello and A. Rahman, Phys. Rev. Lett. **45**, 1196 (1980).
 [2] J. Ray and A. Rahman, J. Chem. Phys. **80**, 4423 (1984).
 [3] J. Ray and A. Rahman, J. Chem. Phys. **82**, 4243 (1985).
 [4] R. Najafabadi and S. Yip, Scripta Metallurgica **17**, 1199 (1983).
 [5] K. W. Wojciechowski and A. C. Brańka, Phys. Lett. A **134**, 314 (1988).
 [6] A. C. Brańka and K. W. Wojciechowski, Mol. Phys. **78**, 1513 (1993).
 [7] J. Lill and J. Broughton, Phys. Rev. B **49**, 11619 (1994).
 [8] D. Frenkel and B. Smit, *Understanding Molecular Simulation*

(Academic Press, London, 2002), 2nd ed.
 [9] S. Pronk, D. A. Fletcher, and P. L. Geissler, in preparation (2008).
 [10] J. Marko and E. Siggia, Macromolecules **28**, 8759 (1995).
 [11] For *NPT* simulations we are not restricted to choosing a rectangular box, but can choose any unit cell that is scaled by a vector l_i ; the rectangular case was chosen here for notational convenience.